SINGLE METALENS FOR GENERATING POLARIZATION AND PHASE SINGULARITIES LEADING TO A REVERSE FLOW OF ENERGY

VICTOR V. KOTLYAR,[1,2] ANTON G. NALIMOV[1,2], SERGEY S. STAFEEV[1,2] AND LIAM O'FAOLAIN[3,4]

[1]*Image Processing Systems Institute of RAS – Branch of the FSRC "Crystallography and Photonics" RAS, 151 Molodogvardeyskaya St., Samara 443001, Russia*

[2]*Samara National Research University, 34 Moskovskoye Shosse, Samara 443086, Russia*

[3]*Centre for Advanced Photonics and Process Analysis, Cork Institute of Technology, Cork, T12 P928, Ireland*

[4]Tyndall National Institute, Cork, T12R5CP, Ireland

Using Jones matrices and vectors, we show that a metasurface-based optical element composed of a set of subwavelength diffraction gratings, whose anisotropic transmittance is described by a matrix of polarization rotation by angle $m\varphi$, where φ is the polar angle, generate an m-th order azimuthally or radially polarized beam, when illuminated by linearly polarized light, or an optical vortex with topological charge m, when illuminated by circularly polarized light. Such a converter performs a spin-orbit transformation, acting similarly to a liquid-crystal half-wave plate. Using the FDTD-aided numerical simulation, we show that uniform linearly or circularly polarized light passing through the above-described optical metasurface with m=2 and then tightly focused with a binary zone plate generates an on-axis near-focus energy backflow comparable in magnitude with the incident energy. Notably, the magnitude of the reverse energy flow is shown to be the same when focusing a circularly polarized optical vortex with topological charge m=2 and a light beam with the second-order polarization singularity.

Key words: optical vortex, polarization singularities, energy backflow, metalens.

Introduction

Optical vortex beams [1], which are characterized by a spiral phase function, have been known for a long time, continuing to attract much attention due to their peculiar properties during propagation [2] and many novel applications. Vortex beams, which carry orbital angular momentum, may find uses in telescopes for exoplanet detection [3] and optical tweezers and spanners for micromanipulation [4, 5, 6], for transferring angular momentum to microparticles [7] and increasing the data carrying capacity of fiber-optic communication systems [8], also showing promise for quantum informatics [9, 10] and high-resolution electron microscopy [11]. One more potential application of optical vortices is associated with the phenomenon of the negative propagation of energy, in which an energy backflow occurs in the opposite direction of the propagation of light [12]. It has been numerically shown [12] that when illuminating a spiral phase plate by a circularly polarized vortex beam, a near-axis backflow of light energy occurs in the sharp focus. The effect of the negative propagation of energy has previously been reported and was shown to occur in superposition of two arbitrary light fields with different projections of the wave-vector onto the longitudinal axis [13]. In some regions of the cross-section of such superposition of light fields, the force exerted upon a microparticle has been shown to be directed oppositely to the beam

propagation. The reverse flow of energy on the optical axis has been shown to occur in the focus of a metalens [14]. The negative propagation of energy has been observed in a vector Bessel beam with fractional topological charge [15]. The said light beam is actually a linear combination of a countable number of conventional Bessel modes. Theoretical relationships to describe the energy flow characteristics given by the Poynting vector of X-beams and necessary conditions for the formation of a reverse energy flow have been derived [16]. Presence of the energy backflow in the cross-section of a non-paraxial accelerating 2D Airy beam has also been demonstrated [17]. Conditions to be imposed on a light field, enabling a quantum backflow and optical retro-propagation to occur locally have been theoretically deduced [18]. Thus, we can see that circularly polarized laser vortex beams are a popular instrument for generating regions in an electromagnetic field with an energy backflow.

Hypothetically, light fields with phase and polarization singularities, which form in free space multiply connected vortex knots [19, 20], may also have regions of the negative propagation of light or the energy backflow.

Recent trends have seen the increasing use of optical metasurfaces for generating laser beams with tailored properties [21-25]. Optical metasurfaces, which represent a nanostructured 100-200-nm metal/semiconductor/dielectric film with a subwavelength feature size may be in the form of an nanorod array [24, 25] or subwavelength binary diffraction gratings [23]. The nanorods, or diffraction grating grooves, are specifically arranged on the metasurface so as to simultaneously control in a desired way the amplitude, phase, and polarization of incident light at each point of the metasurface.

Metasurface-aided optical elements based on varying-thickness catenary arrays in a golden film and bilayer geometric metasurfaces [26, 27], as well as those based on square-split-ring (SSP) nanoantennae or non-parallel double-slit arrays [28,29] have been proposed. A graphene-assisted all-optical tunable Mach-Zehnder interferometer based on microfiber has been reported [30]. Many of such metasurfaces have been utilized in a teraherz bandwidth. As a rule, the said metasurfaces are illuminated by incident fields with tailored characteristics.

In this connection, a question arises whether it is possible to design a metasurface that would be capable of alternately generating a light field with polarization or phase singularity under different illumination.

In this work, we show theoretically and numerically that a combined metalens composed of a binary zone plate with a near-unity NA and an array of subwavelength binary diffraction gratings acting as half-wave plates by rotating the polarization vector of the incident beam by angle $m\varphi$, generate a converging cylindrical vector beam of the m-th order when illuminated by linearly polarized light, or a phase vortex carrying the topological charge m when illuminated by circularly polarized light. In the sharp focus of the converging light beam, a reverse flow of light energy occurs comparable in magnitude with the incident energy.

A metasurface to generate light fields with singularity

It has been known that metasurface-based photonic elements [19, 23, 31-33] containing subwavelength diffraction gratings synthesized in a thin transparent film can operate as local half-wave plates if the diffraction grating parameters provide a phase shift by π between the incident TE- and TM-waves. For the wave emerging from such gratings to be inhomogeneously polarized, their grooves need to have a varied tilt over the metasurface according to a desired pattern of the polarization vector direction [23]. Thus, the metasurface-based half-wave plate rotates the polarization vector by an angle of 2θ, where θ is the angle between the grating grooves and the linear polarization vector of incident light. Such a half-wave plate (subwavelength diffraction grating) is described by a rotation matrix $R(\varphi)$ for the rotation angle $\varphi=2\theta$:

$$R(\varphi)=\begin{pmatrix}\cos\varphi & -\sin\varphi\\ \sin\varphi & \cos\varphi\end{pmatrix}. \quad (1)$$

May there be a metasurface that rotates the polarization vector parallel to the *x*-axis by an angle of $m\varphi$ (*m* is a positive integer) at any point found on a ray drawn from the origin to the *x*-axis. The transmittance of such a metarsurface depends only on the polar angle:

$$R_m(\varphi)=\begin{pmatrix}\cos m\varphi & -\sin m\varphi\\ \sin m\varphi & \cos m\varphi\end{pmatrix}. \quad (2)$$

Below, the metasurface with transmittance (2) is shown to have a multiple functionality, being capable of generating both light fields with the *m*-th order polarization singularity and vortex light fields with the topological charge *m*.

Thus, it can be inferred that the optical metasurface in Eq. (2), which can be referred to as a metasurface-assisted polarization converter (MPC), has similar functionality to a half-wave plate [34], which converts the incident wave into a radially or azimuthally polarized wave, also acting as a spiral phase plate [35] by generating a vortex light field with topological charge *m.* Actually, the MPC converts an incident TE-wave into an *m*-th order radially polarized output light field:

$$R_m(\varphi)\left|TE\right\rangle=\left|RP,m\right\rangle, \quad (3)$$

where

$$\left|TE\right\rangle=\begin{pmatrix}1\\0\end{pmatrix},\quad \left|RP,m\right\rangle=\begin{pmatrix}\cos m\varphi\\ \sin m\varphi\end{pmatrix}. \quad (4)$$

With a normal plane TM-wave incident on the MPC, at the output is an *m*-th order azimuthally polarized wave:

$$R_m(\varphi)\left|TM\right\rangle=\left|AP,m\right\rangle, \quad (5)$$

where

$$\left|TM\right\rangle=\begin{pmatrix}0\\1\end{pmatrix},\quad \left|AP,m\right\rangle=\begin{pmatrix}-\sin m\varphi\\ \cos m\varphi\end{pmatrix}. \quad (6)$$

When illuminated by a plane left-circular polarized wave, the spin-orbit interaction will lead to a left-circular polarized optical vortex with the topological charge *m* emerging from the MPC (2):

$$R_m(\varphi)\left|LCP\right\rangle=e^{im\varphi}\left|LCP\right\rangle, \quad (7)$$

where

$$\left|LCP\right\rangle=\frac{1}{\sqrt{2}}\begin{pmatrix}1\\-i\end{pmatrix}. \quad (8)$$

Finally, an incident right-circular polarized plane wave is converted by the MPC into the emerging right-circular polarized optical vortex with the topological charge $-m$:

$$R_m(\varphi)\left|RCP\right\rangle=e^{-im\varphi}\left|RCP\right\rangle, \quad (9)$$

where

$$\left|RCP\right\rangle=\frac{1}{\sqrt{2}}\begin{pmatrix}1\\i\end{pmatrix}. \quad (10)$$

The above analysis leads to a very interesting corollary. Let us, first, remind that the on-axis near-focus backflow of light energy was shown to occur when sharply focusing (i) a left-circular polarized optical vortex with m=2 [36, 37] or (ii) a second-order azimuthally polarized light wave

[38]. As can be seen from Eqs. (3) - (10), all four varieties of the light field that result in an on-axis energy backflow upon sharp focusing can be generated by means of a single optical element comprising the metasurface in Eq. (2) at m=2. From Eq. (7) it also follows that the (sequential) joint use of a spiral phase plate with topological charge n and an m-th order MPC results in their orders being summed up:

$$e^{in\varphi}R_m(\varphi)\left|LCP\right\rangle = e^{i(m+n)\varphi}\left|LCP\right\rangle. \tag{11}$$

Let us also recall that in Ref. [34], by way of demonstrating the spin-orbit intrcaction, the birefringent liquid crystal plate was interpreted as an anisotropic medium, which was described by a somewhat different matrix and shown to be capable of generating an optical vortex, performing left-to-right circular polarization conversion, unlike grating (7):

$$R'_m(\varphi)\left|LCP\right\rangle = e^{im\varphi}\left|RCP\right\rangle, \tag{12}$$

$$R'_m(\varphi) = \begin{pmatrix} \cos m\varphi & \sin m\varphi \\ \sin m\varphi & -\cos m\varphi \end{pmatrix}. \tag{13}$$

Note that the light fields (3), (7), and (9) are connected via a linear relationship:

$$\left|RP,m\right\rangle = e^{im\varphi}\left|LCP\right\rangle/\sqrt{2} + e^{-im\varphi}\left|RCP\right\rangle/\sqrt{2}, \tag{14}$$

from which the backflow of energy is seen to be the same for the fields with phase and polarization singularities.

Below, using the FDTD-aided simulation (Finite Difference Time Domain), we show that at m=2, the MPC (2) generates an energy backflow in the sharp focus at any type of illumination (TE- and TM-waves, left- and right-circular polarized waves). We are going to show that with all other conditions being the same, the energy backflow in non-vortex and vortex beams is the same in magnitude.

Focusing a field with polarization singularity

In this section, the generation and focusing of a second-order cylindrically polarized light field is numerically simulated. In this field, the E-vector is described by Jones vector:

$$\mathbf{E} = \left|AP, m=2\right\rangle. \tag{15}$$

Projections *Ex* and *Ey* of the electric vector are shown in Fig. 1.

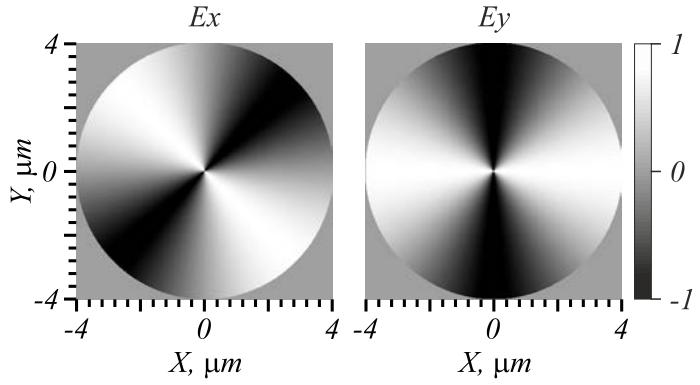

Fig. 1. Projections of the E-vector on the X- and Y-axes: the maximum value is marked in white (+1), the minimal value - in black (-1), and the zero value is marked in grey.

The polarization pattern of the field is depicted in Fig. 2, with a unitary intensity assumed across the entire field.

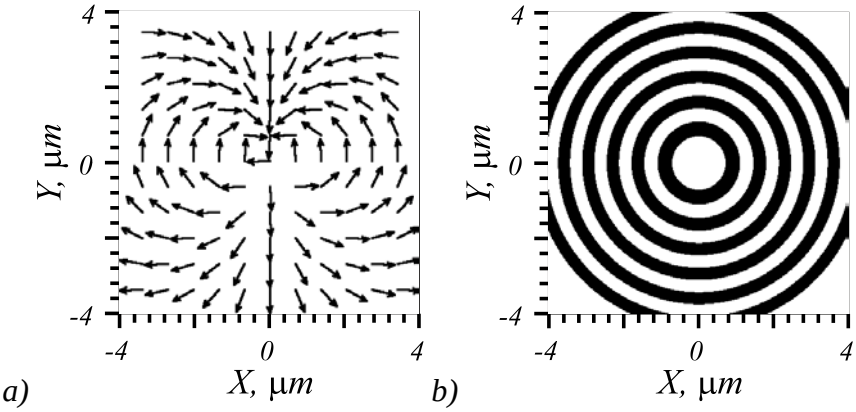

Fig. 2. Pattern of polarization states in the field in Eq. (15) (a) and the Fresnel zone plate used for focusing of the light (b).

Figure 3 depicts the result of focusing the beam of Eq. (15) from Fig. 2a using a binary zone plate (Fig.2b). Shown in Fig. 3 a,b are two-dimensional patterns of the intensity:

$$I = I_x + I_y + I_z = |E_x|^2 + |E_y|^2 + |E_z|^2 \tag{16}$$

and the longitudinal component S_z of the Poynting vector

$$\mathbf{S} = \frac{1}{2}\mathrm{Re}\left[\mathbf{E} \times \mathbf{H}^*\right] \tag{17}$$

in the focal plane (z=600 nm). Shown in Fig. 3 c,d are profiles of the intensity and Pointing vector along the X- and Y-axes. Using an FDTD-aided approach, we numerically simulated the focusing of a beam with polarization singularity (Eq. (15)) with a six-ring binary zone plate on the assumption of the incident wavelength λ=633 nm, focal length f=λ, and a λ/30 increment of the simulation grid on all three coordinates. The field and the zone plate were limited by a 8-μm circular aperture.

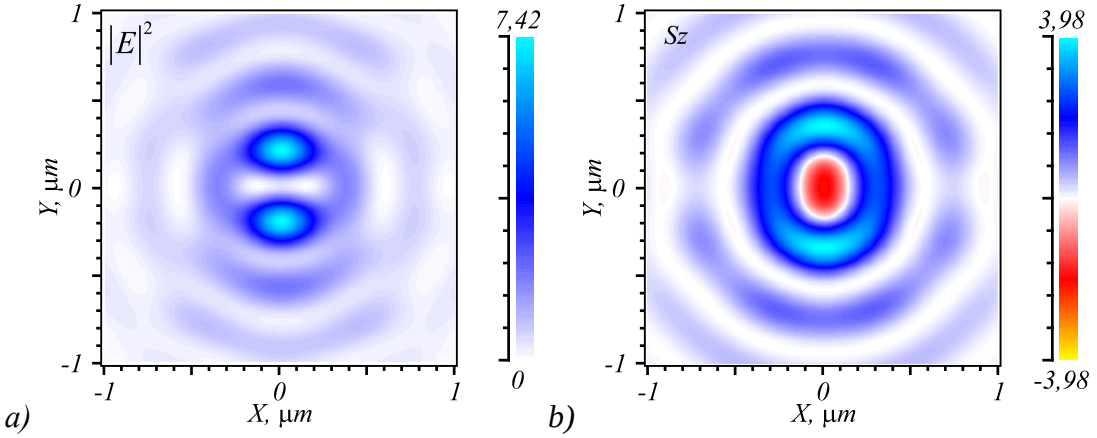

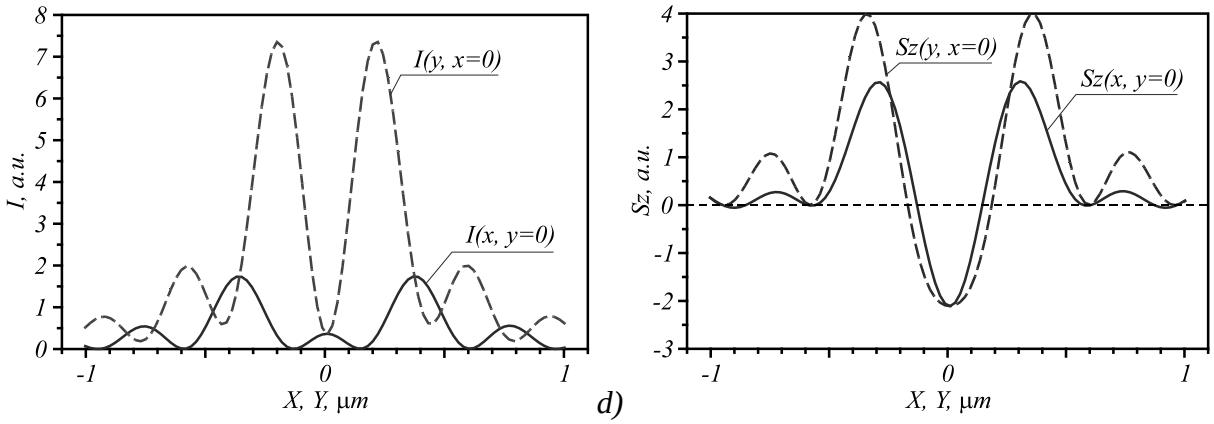

c) d)

Fig. 3. Intensity I of the light field (a,c) and longitudinal component S_z of the Poynting vector (b,d) in the focal plane 0.6-μm behind the zone plate.

It is seen from Fig. 3d that when focusing the field of interest, an on-axis energy backflow occurs in the focal spot.

A metalens for the simultaneous polarization conversion and focusing of light

The idea is that the MPC in Eq. (2) and a focusing binary zone plate may be combined into a single metalens. The individual sectors of the metalens are composed of binary subwavelength gratings. A procedure for calculating optimal parameters (such as the microrelief depth, the period and fill-factor of the grating), enabling the polarization vector to be rotated by a desired angle was described in detail in an earlier work by the present authors [23]. Presented in Fig. 4a is the external appearance of a MPC composed of subwavelength 16-sector binary diffraction gratings whose transmittance is described by matrix (2).

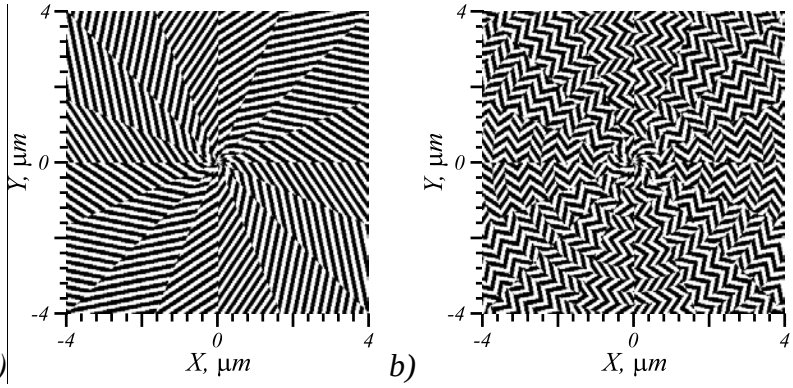

a) b)

Fig. 4. (a) Optical metasurface to generate a phase or polarization vortex and (b) a combined metalens to simultaneously generate and focus a polarization vortex.

Shown in Fig. 4b is a metalens combining the transmittance of the MPC in Fig. 4a and a binary zone plate with near-unity NA (Fig.2b). The metalens is composed of 16 sectors, in which the diffraction gratings alternate according to the zones of a Fresnel zone plate with the focal length f=λ: with the polarization vector in each subsequent zone rotating by π relative to the previous zone. Note that on the zone boundary, the grooves of adjacent diffraction gratings are mutually perpendicular. Putting the refractive index of the metasurface to be n=4.352+0.486i (amorphous silicon), we find that the optimal microrelief height is 120 nm. The gratings have a 200-nm period. The metalens is built on the basis of the optical metasurface in Fig. 4a, whose transmittance is described by matrix (2). If the MPC in Fig. 4a is illuminated by a linearly polarized plane wave, the emerging field at a wavelength distance behind the metasurface will be described by the intensity and polarization vector patterns shown in Fig. 5.

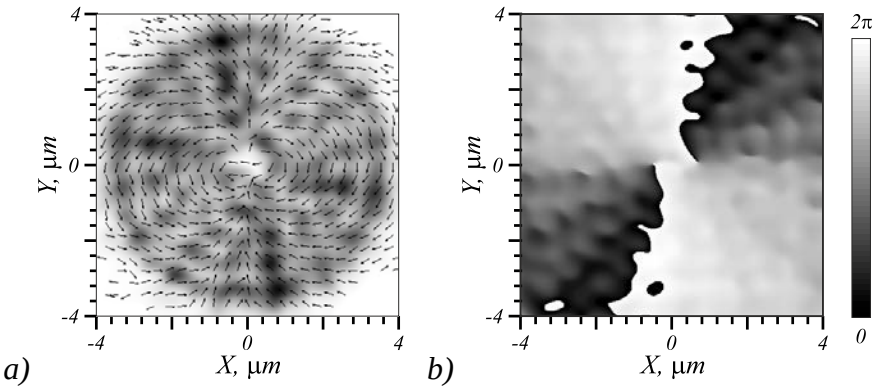

Fig. 5. (a) The intensity of light (negative) emerging from the optical metasurface shown in Fig. 4a для линейно-поляризованного падающего поля (Ex=1, Ey=0). The polarization vectors are marked with arrows and (b) Phase of a light field transmitted by the metasurface in Fig. 4a for a left-circular polarized incident beam.

From Fig. 5a, the intensity of light emerging from the metasurface-assisted polarization converter is seen to be non-uniform because the amount of light energy passing through different metasurface segments is different. Note that rotating the polarization pattern in Fig. 5 by 180 degrees yields the pattern in Fig. 2. It is also worth noting that being non-vortex, the light field in Fig. 5 has a constant phase. Shown in Fig. 5b is the phase of the light field immediately behind the metalens in Fig. 4a upon illumination by a circularly polarized plane wave. The emerging field has a spiral phase characterized by two phase jumps of 2π (Fig. 5b), suggesting the generation of a circularly polarized optical vortex with the topological charge +2, the polarization state being not indicated in Fig. 5b.

Figure 6 depicts results of the metalens-aided (Fig. 4b) focusing of a linearly polarized plane wave limited by a 8-μm aperture, in a similar way to the previous example.

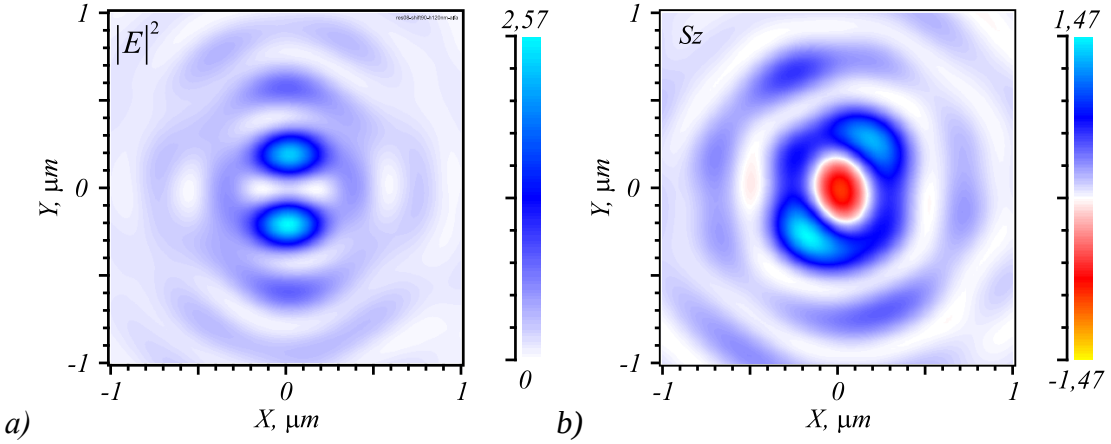

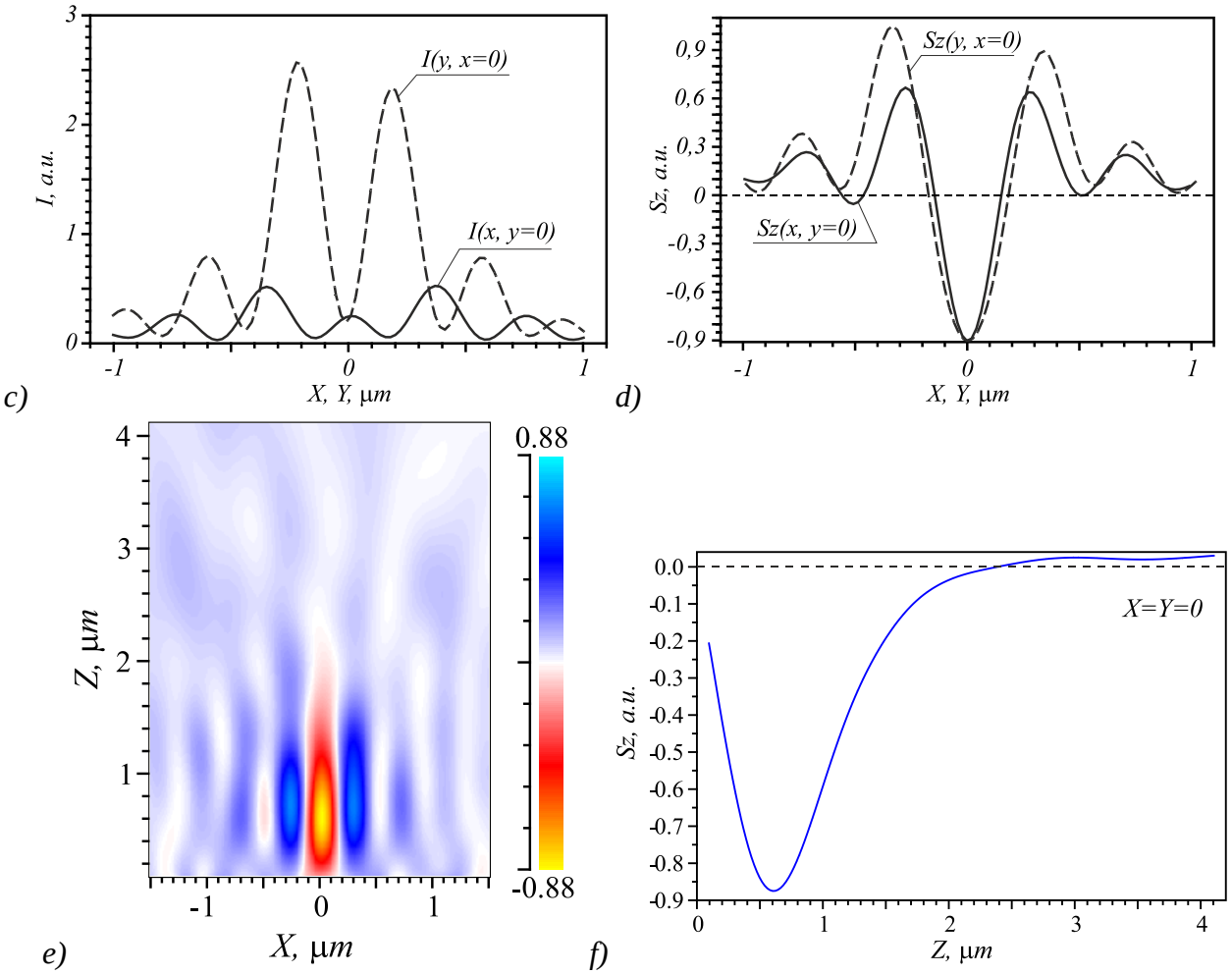

Fig. 6. (a) Intensity of light I and (b) longitudinal projection Sz of the Poynting vector in the focal plane 0.6-μm behind the metalens (Fig. 4b) and (c,d) their respective profiles drawn through the center of the focal spot for a linearly polarized incident wave, (e) the longitudinal pattern of the projection Sz of the Poynting vector in the XZ-plane, and (f) its on-axis profile.

From Fig. 6b, the pattern of the on-axis projection of the Poynting vector in the focal plane is seen to be rotated clockwise by some angle relative to an ideal pattern in Fig. 3b. This is related to the inhomogeneous distribution of light transmitted by the metalens and light-conversion errors introduced by separate metalens sectors (Fig. 5). Meanwhile, the rotation of the linear polarization vector is not a contributing factor here because the said rotation results in the both patterns (Fig. 6a and Fig. 6b) being rotated by the same angle. From Figs. 6 e,f, the magnitude of the energy backflow is seen to be maximum at a distance of ~ 600 nm behind the metalens surface, with its on-axis length at full-width of half-maximum intensity measuring ~1 μm.

The energy backflow at the center of the focal spot is seen to occur in both cases (Fig. 3d and Fig. 6d). In the XY-plane, the region of the energy backflow is in the form of an ellipse with on-axis measurements of 0.27 μm and 0.35 μm for a 0.633-μm incident wave. When focusing with the metalens of Fig. 4b, the projections of the Poynting vector along the *X*- and *Y*-axes are unsymmetrical, which may be owing to a different efficiency of polarization conversion depending on the rotation vector of the E-field.

In magnitude, the energy backflow in Fig. 3d is seen to be nearly twice that in Fig. 6d. The reason is that the metalens of Fig. 4b has the energy efficiency of about 30%.

Comparison of magnitudes of the energy backflow for beams with polarization and phase singularity

This section deals with a comparative numerical simulation. Shown in Figs. 7 and 8 are patterns and respective profiles of the intensity *I* and longitudinal component of the Poynting vector *Sz* in a sharp focus generated by the metalens of Fig. 4b under illumination by a left-circular (Fig. 7) and right-circular (Fig. 8) polarized plane wave. Figures 7 and 8 suggest that in both cases an on-axis energy backflow occurs at the center of the focal spot. From the comparison of the maximum absolute values of the energy backflow for the three examples above (0.9 in Fig. 6d, 1.0 in Fig. 7d, and 0.83 in Fig. 8d), we can see that when focusing a left-circular polarized optical vortex with topological charge 2 and an optical beam with second-order polarization singularity, the energy backflows are nearly the same in magnitude.

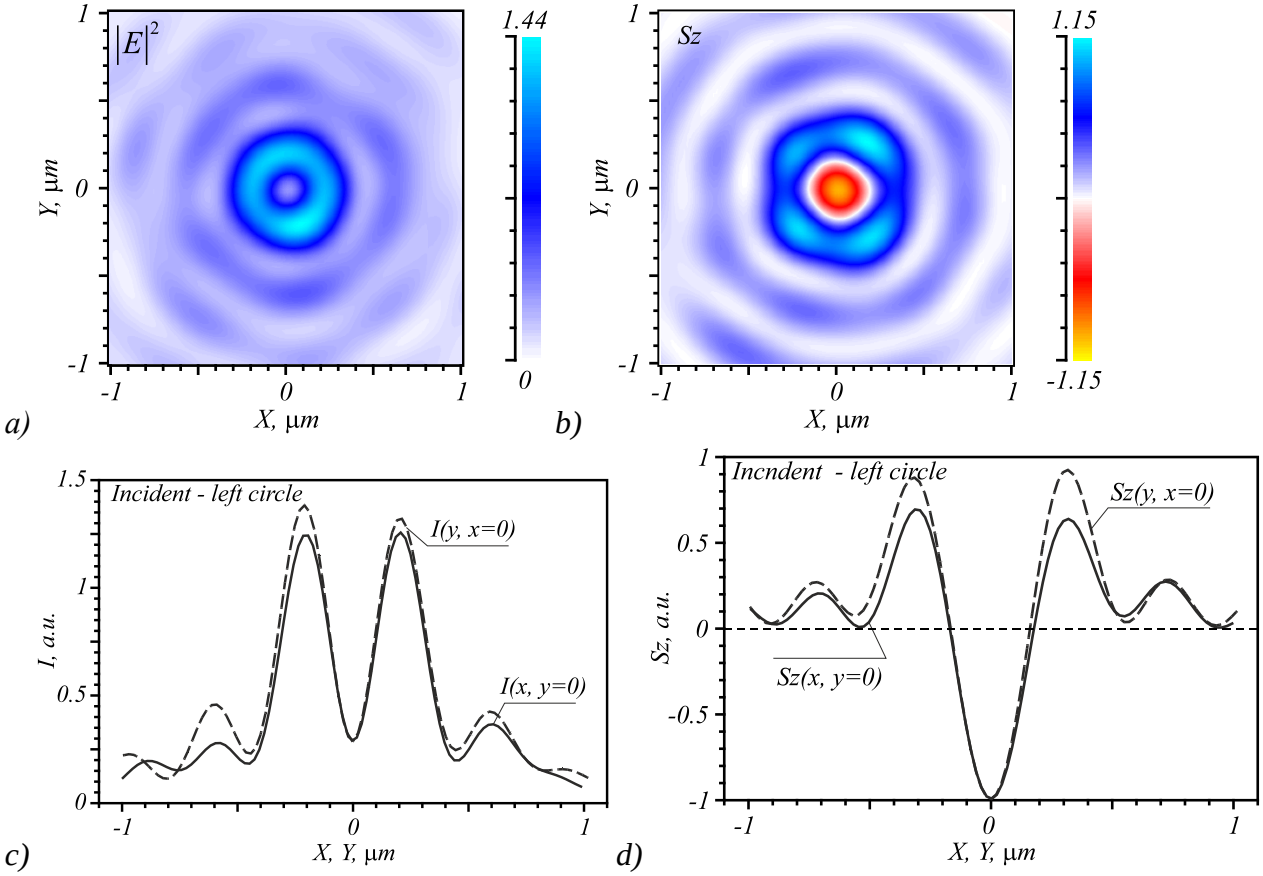

Fig. 7. (a) Intensity of light I and (b) longitudinal projection of the Poynting vector Sz in the focal plane 0.6-μm behind the metalens (fig. 4b) and (c,d) their respective profiles drawn through the center of the focal spot for a left-circular polarized incident wave.

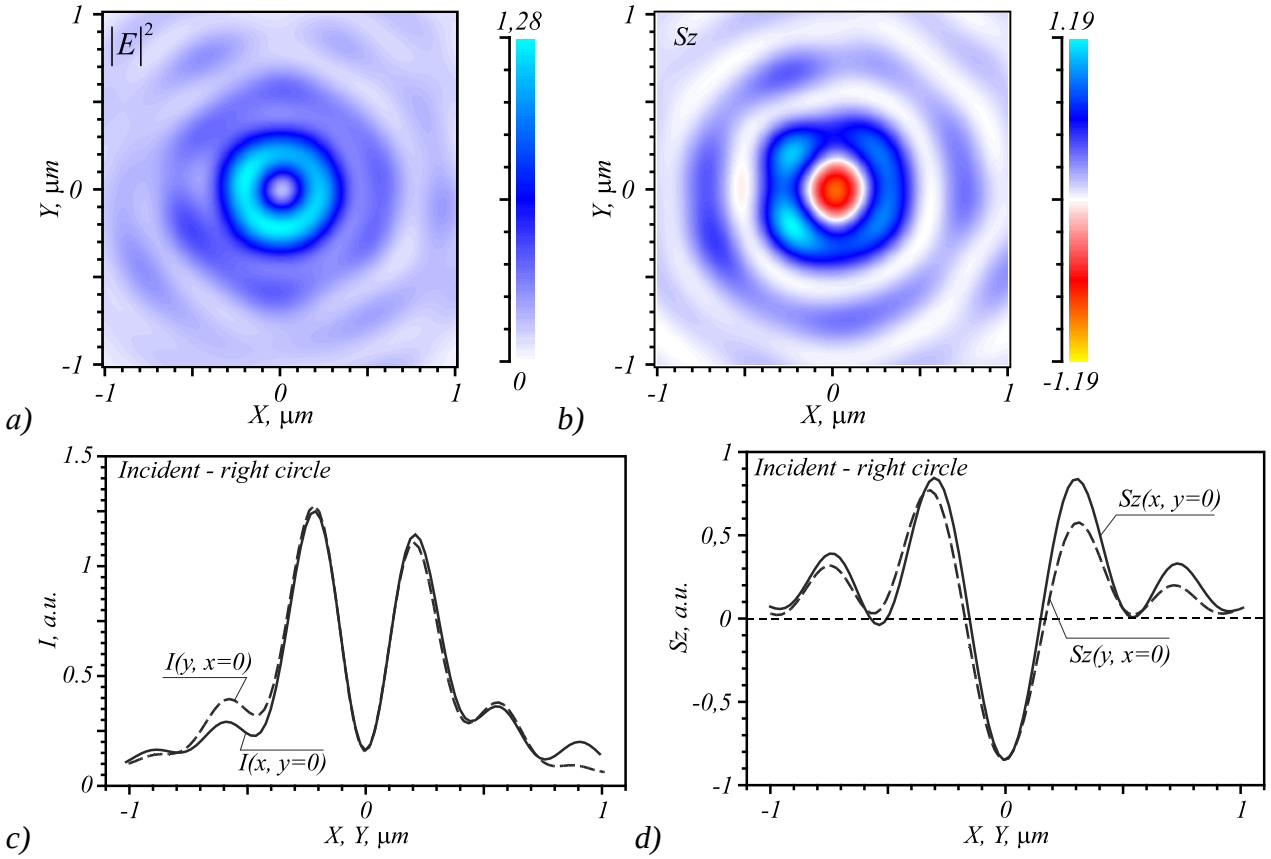

Fig. 8. (a) Intensity of light I and (b) longitudinal projection Sz of the Poynting vector in the focal plane 0.6-μm away from the metalens (fig. 4b) and (c,d) their respective profiles drawn through the center of the focal spot for a right-circular polarized incident wave.

Fabrication of a metalens

The metalens was fabricated using electron beam lithography (Fig.9). A 130-nm-thick amorphous silicon film (a-Si) (with refractive index n=4.35 + i0.486) was deposited on a transparent pyrex substrate (with refractive index n=1.5) coated with a 320-nm-thick PMMA resist, and baked at a temperature of 180C°. The thickness of the resist was chosen to give a combination of good etch resistance and high-resolution patterning. To prevent charging, the surface was sputtered with a gold layer 15 nm in thickness. A binary template was transferred onto the resist surface using a 30 kV electron beam. The specimen was developed in water blended with isopropanol in the ratio 3:7, and the template was then transferred from the resist into an a-Si film, using reactive ion etching in a gaseous atmosphere of CHF_3 and SF_6. The aspect ratio of the etch rate of the material and the photomask was found to be 1:2.5. As a result of this process, the gold was completely washed out from the PMMA surface. An electron microscope image of the metalens is shown in Fig. 9a.

The focusing of light by the fabricated spiral metalens was investigated experimentally using a scanning near-field optical microscope (Ntegra Spectra, NT-MDT). The intensity distribution is shown in Fig. 9b. It can be seen that the difference between the intensities of two central lobes is almost two-fold. Therefore, the agreement between the theory (Fig. 6a) and the experiment (Fig. 9b) is just qualitative. The reason may be not just in imperfections of the metalens fabrication process but also in alignment difficulties, because the centers of the focused linearly polarized Gaussian beam and the metalens need to be precisely aligned (Fig. 9b). The authors are planning to conduct a

detailed characterization of the fabricated metalens in a future study. In the meantime, the plots in Fig. 9 should be looked upon as a proof of principle for the metalens fabrication.

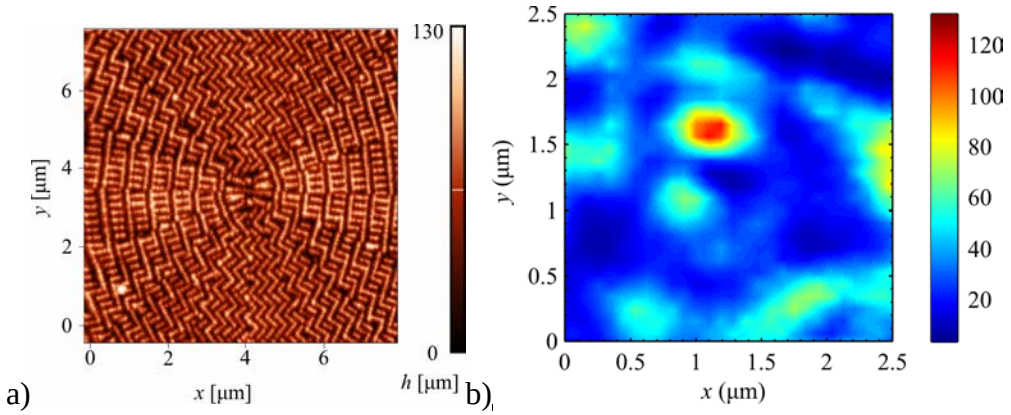

Fig 9: Atomic force microscope images of a spiral metalens in an a-Si film (a) and measured intensity of the focal spot: 2D intensity pattern (b)

A model for generating an on-axis energy backflow in the sharp focus

A rigorous theory that accounts for the generation of an on-axis energy backflow in the focus of an left-circular polarized optical vortex with the topological charge 2 can be found in Ref. [37]. The existence of an on-axis energy backflow in the focus of a metalens can be explained most simply for focusing a second-order azimuthally polarized light field (Fig. 2a). From Fig. 2a, the polarization vectors of the E-field are seen to be directed vertically downwards on the optical axis and vertically upwards on the x-axis. Figure 10 schematically shows the superposition of four plane waves with their polarization vectors directed similarly to the vectors in Fig.2a, though rotated by 90 degrees.

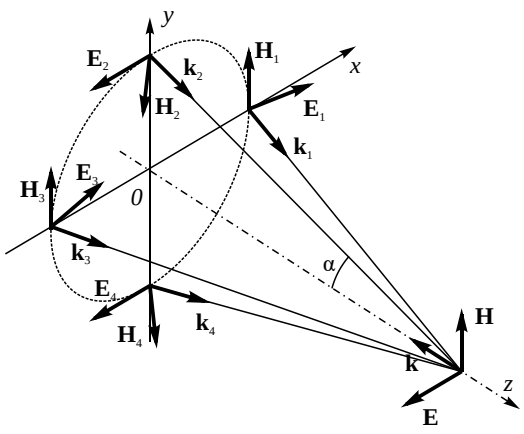

Fig. 10. Schematic of superposition of four linearly polarized plane waves.

For the four plane waves in Fig. 10, the resultant amplitudes of the **E**- and **H**- vectors and the Poynting vector **S**=c**k** on the optical axis (x=y=0) are given by

$$\begin{aligned}
&\mathbf{E}(x=y=0)=\mathbf{E}_1+\mathbf{E}_2+\mathbf{E}_3+\mathbf{E}_4=-2\mathbf{e}_x(1-\cos\alpha)\exp(ikz\cos\alpha),\\
&\mathbf{H}(x=y=0)=\mathbf{H}_1+\mathbf{H}_2+\mathbf{H}_3+\mathbf{H}_4=2\mathbf{e}_y(1-\cos\alpha)\exp(ikz\cos\alpha),\\
&\mathbf{S}(x=y=0)=-2\mathbf{e}_z(1-\cos\alpha)^2,
\end{aligned} \tag{18}$$

where **k** is the wavevector of the light field and α is the angle of incidence of plane waves on the optical axis. In Eq. (18), the unit vectors ($\mathbf{e}_x$, $\mathbf{e}_y$, $\mathbf{e}_z$) define a right-handed triplet in the Cartesian coordinates, suggesting that the vectors **-S=-***c***k**, **E**, **H** form right-handed triplet vectors, defining a plane wave propagating along the optical axis in the negative direction.

Conclusion

In this work, we have designed, studied, and fabricated a multi-sector metalens in a thin transparent film (e.g. amorphous silicon). Boasting a double functionality, the metalens is capable of (i) converting an incident linearly polarized wave into an *m*-th order azimuthally/radially polarized wave and an incident circularly polarized plane wave into a circularly polarized optical vortex with the topological charge *m* and (ii) generating a sharp focus of the transmitted beam at an incident-wavelength distance behind the metalens. It has been numerically shown that at *m*=2, for both the polarization and phase singularities, the on-axis near-focus reverse flow of light energy is comparable in magnitude with the incident energy. In magnitude, the reverse energy flow has been shown to be nearly the same when focusing a phase vortex and a beam with polarization singularity. Theoretically, it follows from Eq. (14) that the magnitude of the non-vortex energy backflow should exactly equal that of the vortex energy backflow.

Acknowledgements

The work was partly funded by the Russian Science Foundation under grant # 18-19-00595 ("A metasurface for generating light fields with singularities), RF Ministry of Science and Higher Education under a state contract awarded to FRDC "Crystallography and Photonics" of the RAS ("Focusing a field with polarization singularity"), and Russian Foundation for Basic Research under grant # 18-29-20003 ("A metalens for simultaneous polarization conversion and focusing of light").

References

[1]Nye JF, Berry MV. Dislocations in wave trains. Proc. R. Soc. London Ser. A, 1974; 336: 165–90.

[2]Soskin MS, Vasnetsov MV. “Singular optics,” in Progress in Optics, E. Wolf, ed. (Elsevier, 2001), Chap. 4, pp. 219–276.

[3]Grover AS, Jr. The optical vortex coronagraph. J. Opt. A, 2009; 11: 094022.

[4]Gahagan KT, Swartzlander GA. Optical vortex trapping of particles. Opt. Lett., 1996; 21: 827–9.

[5]Gecevičius M, Drevinskas R, Beresna M, Kazansky PG. Single beam optical vortex tweezers with tunable orbital angular momentum. Appl. Phys. Lett., 2014; 104: 231110.

[6]Simpson NB, Dholakia K, Allen L, Padgett MJ. Mechanical equivalence of spin and orbital angular momentum of light: an optical spanner. Opt. Lett., 1997; 22: 52–4.

[7]Volke-Sepulveda K, Garces-Chavez V, Chavez-Cerda S, Arlt J, Dholakia K. Orbital angular momentum of a high-order Bessel light beam. J. Opt. B, 2002; 4: S82–S89.

[8]Thidé B, Then H, Sjöholm J, Palmer K, Bergman J, Carozzi TD, Istomin YN, Ibragimov NH, Khamitova R. Utilization of photon orbital angular momentum in the low-frequency radio domain. Phys. Rev. Lett., 2007; 99: 087701.
[9]Bandyopadhyay A and Singh RP. Wigner distribution of elliptical quantum optical vortex. Opt. Commun., 2011; 284: 256–61.
[10] Bandyopadhyay A, Prabhakar S, and Singh RP. Entanglement of a quantum optical elliptic vortex. Phys. Lett., 2011; A375: 1926–9.
[11] McMorran BJ, Agrawal A, Anderson IM, Herzing AA, Lezec HJ, McClelland JJ, and Unguris J. Electron vortex beams with high quanta of orbital angular momentum, Science, 2011; 331: 192–5.
[12] Stafeev SS, Nalimov AG. Longitudinal component of the Poynting vector of a tightly focused optical vortex with circular polarization. Computer Optics 2018; 42(2): 190-196. DOI: 10.18287/2412-6179-2018-42-2-190-196.
[13] Sukhov S, Dogariu A. On the concept of "tractor beams". Opt. Lett., 2010; 35: 3847-3849.
[14] Kotlyar VV, Nalimov AG. A vector optical vortex generated and focused using a metalens. Computer Optics, 2017; 41(5): 645-653.
[15] Mitri FG. Reverse propagation and negative angular momentum density flux of an optical nondiffracting nonparaxial fractional Bessel vortex beam of progressive waves. J. Opt. Soc. Am. A, 2016; 33: 1661-7.
[16] Salem MA, Bagci H. Energy flow characteristics of vector X-wave. Opt. Express, 2011; 19: 8526-32.
[17] Vaveliuk P, Martinez-Matos O. Negative propagation effect in nonparaxial Airy beams. Opt. Express, 2012; 20: 26913-21.
[18] Berry MV. Quantum backflow, negative kinetic energy, and optical retro-propagation. J. Phys. A: Mathem. & Theor, 2010; 43: 415302.
[19] Irvine WNM, Boumeester D. Linked and knotted beams of light. Nature Physics, 2008; 4: 716-20.
[20] Sugic D, Dennis MR. Singular knot bundle in light. J. Opt. Soc. Am. A, 2018; 35(12): 1987-1999.
[21] Yu N, Genevet P, Kats MA, Avieta F, Terienne JP, Capasso F, Gaburro Z. Light propagation with phase discontinuities: generalized lows of reflection and refraction. Science, 2011; 334(6054): 333-7.
[22] Arbabi A, Horie Y, Bagheri M, Faraon A. Dielectric metasurfaces for complete control of phase and polarization with subwavelength spatial resolution and high transmission. Nat. Nanotechnology, 2015; 10(11): 937-43.
[23] Kotlyar VV, Nalimov AG, Stafeev SS, Hu G, O'Faolain L, Koltyar MV, Gibson D, Song S. Thing high numerical aperture metalens. Opt. Express, 2017; 25(7): 8158-67.
[24] Tian S, Guo H, Hu J, Zhuang S. Dielectric longitudinal bifocal metalens with adjustable intensity and high focusing efficiency. Opt. Express, 2019; 27(2): 680-8.
[25] Park CS, Koirala I, Gao S, Shrestha VR, Lee SS, Choi DY. Structural color filter based on an all-dielectric metasurface exploiting silicon-rich silicon nitride nanodisks. Opt. Express, 2019; 27(2): 667-78.
[26] Pu M, Li X. Ma X., Wang Y, Zhao Z, Wang C, Hu C, Gao P, Huang C, Ren H, Li X, Qin F, Yang J, Gu M, Hong M, Luo X. Catenary optics for achromatic generation of perfect optical angular momentum. Sci. Adv., 2015; 1: e1500396.

[27] Guo Y, Ma X, Pu M, Li X, Zhao Z, Luo X. High-efficiency and wide-angle beam steering based on catenary optical fields in ultrathin metalens. Adv. Opt. Mater., 2018: 1800592.
[28] Wang J, Ma J, Shu Z, Hu Z, Wu X. Terahertz metalens for multifocusing bidirectional arrangement in different dimensions. IEEE Phot. J., 2019; 11(1):4600311.
[29] Shao H, Chen C, Wang J, Pan L, Sang T. Metalenses based on the non-parallel double-slit arrays. J. Phys. D, 2017; 50(38): 384001.
[30] Liu Z, Meng Y, Xiao H, Deng L, Guo X, Liu G, Tian Y. Graphene-assisted all-optical tunable Mach-Zehnder interferometer based on microfiber. Opt. Commun., 2018; 428: 77-83.
[31] Kotlyar VV, Zalyalov OK. Design of diffractive optical elements modulating polarization. Optik, 1996; 103(3): 125-30.
[32] Bomzon Z, Biener G, Kleiner V, Hasman E. Space-variant Pancharatnam-Berry phase optical elements with computer-generated subwavelength gratings. Opt. Lett., 2002; 27(13): 1141-3.
[33] Niv A, Biener G, Kleiner V, Hasman E. Propgation-invariant vectorial Bessel beams obtained by use of quantized Pancharatnam-Berry phase optical elements. Opt. Lett., 2004; 29(3): 238-40.
[34] Marrucci L, Manzo C, Paparo D. Optical spin-to-orbital angular momentum conversion in inhomogeneous anisotropic media. Phys. Rev. Lett., 2006; 96: 163905.
[35] Kotlyar VV, Khonina SN, Uspleniev GV, Shinkarev MV, Soifer VA. The phase rotor filter. J. Modern Optics, 1992; 39(5): 1147-54.
[36] Kotlyar VV, Nalimov AG. Sharp focusing of vector optical vortices using a metalens. Journal of Optics, 2018; 20(7): 075101.
[37] Kotlyar VV, Kovalev AA, Nalimov AG. Energy density and energy flux in the focus of an optical vortex: reverse flux of light energy. Opt. Lett. 2018; 43(12): 2921-4.
[38] Stafeev SS, Nalimov AG, Kotlyar VV. Energy backflow in a focal spot of the cylindrical vector beam. Computer Optics 2018; 42(5): 744-750. DOI: 10.18287/2412-6179-2018-42-5-744-750.